Abdominal Radiology (2019) 44:3432–3440
https://doi.org/10.1007/s00261-019-02105-0

PELVIS

# Validation of SE-EPI-based T2 mapping for characterization of prostate cancer: a new method compared with the traditional CPMG method

Zan Ke[1] · Xu Yan[2] · Xiangde Min[1] · Wei Cai[1] · Peipei Zhang[1] · Huijuan You[1] · Chanyuan Fan[1] · Liang Wang[1]

Published online: 19 June 2019


## Abstract

**Purpose** We aim to compare the results of spin echo–echo planar imaging (SE-EPI)-based T2 mapping with those of the conventional Carr–Purcell–Meiboom–Gill (CPMG) method and to investigate the potential validity of SE-EPI-T2 mapping for the characterization of prostate cancer (PCa).

**Methods** Our retrospective study included 42 PCa patients and 42 noncancer patients who underwent 3.0T MRI with *b* values ranging from 0 to 2000 s/mm$^2$ and echo times (TEs) ranging from 32 to 100 ms before biopsies. Bland–Altman analysis was used to compare the agreement between the two methods. The correlations between CPMG-T2 values and SE-EPI-T2 values at different *b* values were determined by Spearman's rho analysis or Pearson analysis. The Mann–Whitney *U* test and two-sample *t* tests were used to analyze the differences between the cancerous and noncancerous groups.

**Results** Substantial agreement regarding the measurements was observed between the two methods. The average correlation between the CPMG-T2 values and SE-EPI-T2 values was moderate and positive, and the best correlations were found at $b = 200$ s/mm$^2$ in the noncancer group ($r = 0.557$, $P = 0.000$) and at $b = 100$ s/mm$^2$ in the cancer group ($r = 0.537$, $P = 0.000$). In addition, statistically significant differences were found between the noncancer and cancer groups in T2 values and ADC values (diff TEs) ($P = 0.000$).

**Conclusions** Substantial agreement in the measurements was found between the SE-EPI method and CPMG method. SE-EPI-based T2 mapping has potential clinical value for the prostate and can be considered an alternative to the traditional CPMG-T2 mapping method.

**Keywords** Diffusion magnetic resonance imaging · Echo planar imaging · Magnetic resonance imaging · Prostate cancer · T2 mapping

✉ Liang Wang
wang6@tjh.tjmu.edu.cn

Zan Ke
xlydyx@163.com

Xu Yan
xu.yan@siemens.com

Xiangde Min
minxiangde0129@126.com

Wei Cai
280734016@qq.com

Peipei Zhang
1532910664@qq.com

Huijuan You
710161132@qq.com

Chanyuan Fan
2472580729@qq.com

[1] Department of Radiology, Tongji Hospital, Tongji Medical College, Huazhong University of Science and Technology, No. 1095 Jiefang Road, Wuhan 430030, Hubei, China

[2] MR Collaboration NE Asia, Siemens Healthcare, Shanghai 201321, China

## Introduction

Prostate cancer (PCa) remains the largest contributor to new male cancer cases in the United States, and the death toll in 2018 is second only to that of lung/bronchial tumors [1].

Magnetic resonance imaging (MRI) is the preferred imaging method for the prostate and periprostatic structures because this technique provides superior soft-tissue contrast resolution and a smaller field of view with a higher spatial resolution compared to other imaging methods. MRI can also provide more functional information [2–4]. In 2012, the European Society of Urogenital Radiology (ESUR) launched the first Prostate Imaging Reporting and Data System (termed PI-RADS) [5], which was updated in 2015 (called PI-RADS v2) [6]. However, the PI-RADS guideline was based on only a few regular sequences that mostly emphasize qualitative information, which is more dependent on individual subjective perception and evaluation.

T2 mapping is a common functional sequence that measures the T2 values of tissues for quantitative analysis of changes in tissue [7], and some previous studies [8–13] have revealed its potential value in various human tissues and organs, including the prostate [14, 15] where T2 values differ significantly between benign and malignant lesions. However, traditional T2 mapping is based on the Carr–Purcell–Meiboom–Gill (CPMG) method, which uses the spin-echo (SE) sequence. This method is valuable but is not widely used due to its long acquisition time (usually 5–10 min).

Wang et al. [16] reported a study introducing a fast T2-mapping method based on an SE-EPI (echo planar imaging) sequence; this method can acquire matched T2 and apparent diffusion coefficient (ADC) mapping for simultaneous analysis by incorporating T2 mapping into the diffusion-weighted imaging (DWI) scan. Unfortunately, the main limitation of the study was that the authors did not compare the results of the SE-EPI method with those of the conventional CPMG method because the T2 map from the long echo train of the SE-EPI sequence could be affected by T2* effects. Although our studies [17, 18] over the past 2 years have shown a strong correlation between the SE-EPI method and the CPMG method in terms of T2 values, our previous works were solely preliminary explorations with a small number of cases ($n = 28$).

Therefore, we conducted further research using the SE-EPI-based method in this study focusing on the following objectives: (1) include more patients with more lesions; (2) compare correlations between CPMG-T2 values and SE-EPI-T2 values at different b-values; and (3) investigate the effectiveness of T2 values at different b-values and ADC values at different echo times (TEs) in terms of differentiating benign and malignant prostate lesions.

## Materials and methods

### Study design and patient selection

This retrospective study was approved by our institutional review board, and informed consent was obtained from all patients before the examinations. Between January 2016 and November 2016, 123 patients with clinically suspected prostate disease were recruited for this study. All patients underwent prostate MRI using the study protocol and met the following inclusion criteria: (1) no contraindications for MRI scanning; (2) no prior treatment history, including irradiation, cryosurgery, hormonotherapy, radical prostatectomy, or other surgical therapies; and (3) no biopsy examinations within the 6 weeks prior to undergoing MRI. However, only 84 cases were ultimately selected for the data analysis based on the following exclusion criteria: (1) no histopathologically confirmed results ($n = 33$); (2) pathological results showing that the clinically suspected prostate tumor originated from nonprostate tissue ($n = 3$); (3) MRI scans showing serious movement artifacts ($n = 2$); or (4) errors during the original data transfer that prevented further analysis ($n = 1$). Thus, 39 of the initial 123 patients were excluded. The flowchart (Fig. 1) presents more information regarding the patient selection process.

### MRI acquisition

All examinations were performed with a 3.0T MAGNETOM Skyra MRI scanner (Siemens Healthcare, Erlangen, Germany) using an anterior 18-element body coil combined with a posterior spine coil array. An endorectal coil was not used, and all patients were required to evacuate the rectum prior to the MRI exam. A single-shot SE-EPI-based diffusion sequence was applied to acquire the datasets, and the acquisitions were performed in 8 independent sessions with multiple b-values (from 0 to 2000 s/mm$^2$) and multiple TEs (from 32 to 100 ms); the total acquisition time was 13 min 25 s, while each session was mostly less than 3 min (Table 1). The scan sequences also included common transverse T1-weighted turbo spin-echo sequences (slice thickness, 5 mm; TE/repetition time (TR) = 13/807 ms; intersection gap, 0 mm; field of view (FOV), 300 × 356 mm$^2$; matrix, 320 × 240; flip angle, 160°; and scan time, 3 min 6 s), transverse, sagittal, and coronal T2-weighted turbo spin-echo sequences (all with the following parameters: slice thickness, 3 mm; TE/TR range = 104/6500–6874 ms; intersection gap, 0 mm; FOV, 180 × 180 mm$^2$; matrix, 384 × 384; flip angle, 160°; parallel imaging factor, 2; and scan time, 3 min 16 s, 3 min 10 s, and 3 min 7 s, respectively), and traditional transverse CPMG-T2 mapping based on the spin-echo sequence with six echoes and TE times ranging from 10.5

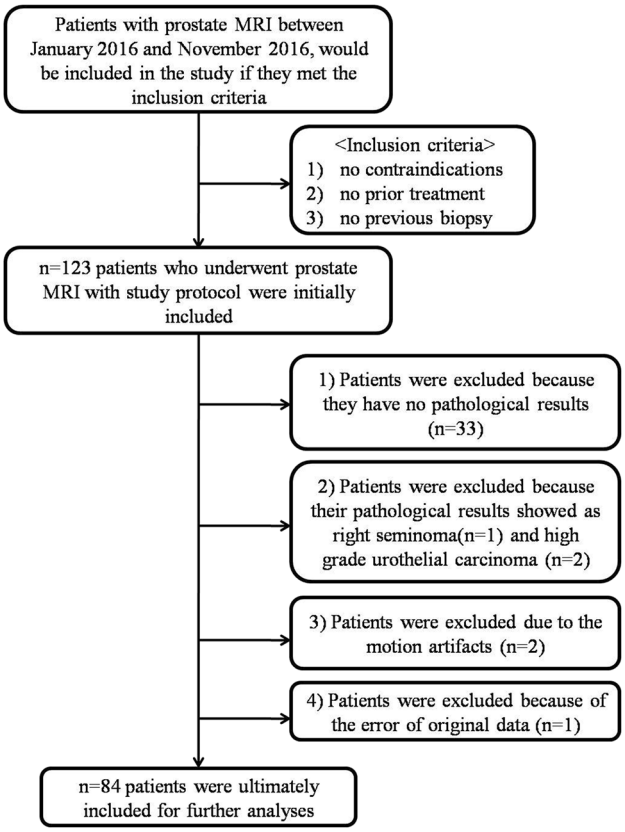


**Fig. 1** Flowchart for patient selection in the present study. *MR*I magnetic resonance imaging

to 63 ms (slice thickness, 3 mm; TR = 2000 ms; intersection gap, 0 mm; FOV, 256 × 256 mm$^2$; matrix, 192 × 256; flip angle, 180°; and scan time, 5 min 16 s).

## Data analysis and T2 mapping calculation

After MRI scanning, all original SE-EPI-T2 mapping images were analyzed according to the PI-RADS v2 guideline [6], and then regions of interest (ROIs) were drawn manually within suspicious cancer and noncancer areas based on DWI images at $b = 1000$ s/mm$^2$, and the ADC map and other T1WI/T2WI scans were used simultaneously as reference images. All ROIs were drawn by one radiologist with 4 years of experience in prostate imaging using in-house developed software. During ROI drawing, the radiologist outlined one ROI of dominant lesion for each patient, and then the results of biopsy were used as the reference standard. In our study, the dominant lesion was defined as a hyperintense region on DWI images with $b = 1000$ s/mm$^2$. For patients with more than one lesion with equal signal strength, the largest suspicious lesion (on diameter) was defined as the dominant lesion [19, 20]. The software calculated the T2 maps of the DWI data at different b-values independently

**Table 1** SE-EPI sequence protocol

| Acquisition[a] | TE(ms) | TR(ms) | *b* value (s/mm$^2$) | FOV (mm$^2$) | Matrix | Acquisition time | NEX | Section thickness (mm) | Slices[b] | iPAT factor |
|---|---|---|---|---|---|---|---|---|---|---|
| 1 | 32 | 4500 | 0 | 171 × 214 | 72 × 90 | 13 s | 1 | 3 | 22 | 2 |
| 2 | 36 | 4500 | 0, 100 | 171 × 214 | 72 × 90 | 27 s | 1 | 3 | 44 | 2 |
| 3 | 40 | 4500 | 0, 20, 40, 60, 100, 200 | 171 × 214 | 72 × 90 | 1 min 21 s | 1 | 3 | 132 | 2 |
| 4 | 54 | 4500 | 0, 20, 40, 60, 100, 200, 500, 1000 | 171 × 214 | 72 × 90 | 1 min 48 s | 1 | 3 | 176 | 2 |
| 5 | 69 | 4500 | 0, 20, 40, 60, 100, 200 | 171 × 214 | 72 × 90 | 3 min 45 s | 3 | 3 | 132 | 2 |
| 6 | 69 | 4500 | 0, 20, 40, 60, 100, 200, 500, 1000, 1500, 2000 | 171 × 214 | 72 × 90 | 2 min 15 s | 1 | 3 | 220 | 2 |
| 7 | 80 | 4500 | 0, 100, 200, 500, 1000, 2000 | 171 × 214 | 72 × 90 | 1 min 48 s | 1 | 3 | 132 | 2 |
| 8 | 100 | 4500 | 0, 100, 200, 500, 1000, 2000 | 171 × 214 | 72 × 90 | 1 min 48 s | 1 | 3 | 132 | 2 |

*TE* echo time, *TR* repetition time, *NEX* number of excitations, *SE* spin echo, *EPI* echo planar imaging, *FOV* field of view

[a]Frequency selective fat saturation was applied on each acquisition

[b]The number of slices on each *b* value is 22 slices

with a linear-least-square fitting method using the following equation:

$$S(b, TEn) = S(b, 0) \cdot \exp(-TEn/T2) \quad (1)$$

The ADC was also calculated with linear-least-square fitting using the following equation:

$$S(b, TEn) = S(0, TEn) \cdot \exp(-b \cdot ADC) \quad (2)$$

where S (b, TEn) is the signal at the n-th TE, and S(b, 0) and T2 are the fitted variables. The mean SE-EPI-T2 values and ADC values of the ROI were then automatically calculated. All algorithms were implemented using Python (https://www.python.org).

The CPMG-T2 mapping images were transferred to a digital workstation (Syngo MultiModality Workplace VE40B; MAGNETOM Skyra, Siemens Healthcare, Erlangen, Germany), and the CPMG-T2 values were calculated automatically when ROI drawing was complete. Each ROI was drawn at the same location (on the same layer) on both the SE-EPI-T2 mapping and CPMG-T2 mapping images. Other clinical patient information was obtained from our own electronic case system.

### Pathological evaluation

All 84 patients underwent a cognitive fusion-targeted biopsy (COG-TB) and systematic transrectal ultrasound (TRUS)-guided prostate biopsy within 7–30 days after the MRI examination to obtain tissue samples for histopathological examination, and all biopsies were performed based on suspicious findings on MRI and/or increased prostate-specific antigen (PSA). Each specimen was individually labeled according to its location and histologically analyzed to determine whether it was cancerous or noncancerous.

### Statistical analysis

SPSS 19.0 (SPSS, Chicago, IL, USA) and MedCalc version 11.4.2.0 (MedCalc statistical software, Mariakerke, Belgium) were used for the data analyses, and all data analyses were performed per lesion. Our data are presented as the mean and standard deviation (SD) and the median and range. The normality and equality of the variances in the parameter value distributions were tested by the Shapiro–Wilk test and Levene's $F$ test. First, Bland–Altman analysis was used to compare the agreement between the two methods. Then we discussed the relationship between the CPMG-T2 values and SE-EPI-T2 values at different b-values. The decision regarding whether to calculate Pearson or Spearman correlation coefficients (represented by "$r$") also depended on whether the data followed a normal distribution. The $r$ values were assessed as follows: 0–0.25, low (if any correlation); 0.25–0.5, weak; 0.5–0.75, moderate; and $r \geq 0.75$, strong. In addition, to analyze the differences between the cancerous and noncancerous groups in terms of the T2 values (diff $b$ values) and ADC values (diff TEs), the Mann–Whitney $U$ test was used when the data did not adhere to a normal distribution. Two-sample $t$ tests were used when the data followed a normal distribution. All statistical tests were two-sided, and $P < 0.05$ was considered statistically significant.

## Results

Our study included 84 patients with a total of 84 lesions (average age 66.5 years, range 31–97 years; Gleason score (GS) range 6–10, mean 7.9; and serum PSA range 0.63–1000 ng/ml, median 14.48 ng/ml). Forty of these patients were diagnosed with benign prostrate hyperplasia (BPH), and 2 patients were diagnosed separately with prostatic abscess and nonspecific granulomatous prostatitis, thus constituting the noncancer group. In addition, 42 patients diagnosed as PCa were incorporated into the study as the cancer group. The patient group characteristics are shown in Table 2.

Bland–Altman plots (some representative examples are shown in Figs. 2 and 3) illustrate the substantial agreement between the two methods in the measurement of T2 values (diff $b$ values) in both the cancer group and noncancer group, and the optimum agreement was found at $b = 20$, 40, 60, 100, and 200 s/mm$^2$. In addition, a summary of quantitative imaging findings is presented in Table 3, the average correlation between the CPMG-T2 values and SE-EPI-T2 values was moderate and positive, and the best correlation was found at $b = 200$ s/mm$^2$ in the noncancer group ($r = 0.557$, $P = 0.000$) and at $b = 100$ s/mm$^2$ in the cancer group ($r = 0.537$, $P = 0.000$). In addition, no statistically significant differences were found at $b = 1000$ and 2000 s/mm$^2$ in the noncancer group ($P = 0.788$ and 0.064) or at $b = 500$, 1000, and 2000 s/mm$^2$ in the cancer group ($P = 0.147$, 0.312, and 0.310).

Table 4 shows the group analysis of T2 values at different $b$ values and ADC values at different TEs. Significant differences in the various $b$ values were found between the noncancer group and the cancer group. The T2 values of the cancer group were lower than those of the noncancer group at $b \leq 500$ s/mm$^2$ but higher than those of the noncancer group at $b = 1000$ and 2000 s/mm$^2$. Besides that, the ADC values of the cancer group were lower than those of the noncancer group at different TEs, and the cancer group and the noncancer group exhibited significant differences among the various TEs. Figures 4 and 5 present examples of original DWI images of BPH and PCa patients at the same $b$ values but with different TEs, revealing significant contrast between the images.

**Table 2** Characteristics of the patients enrolled in this study

| Characteristics | All | Cancer group | Noncancer group |
|---|---|---|---|
| Number of patients | 84 | 42 | 42 |
| Age (years), mean (range) | 66.5 (31.0–97.0) | 69.5 (53.0–97.0) | 63.5 (31.0–91.0) |
| PSA level (ng/ml), median (range) | 14.48 (0.63–1000) | 60.09 (1.51–1000) | 10.54 (0.63–55.23) |
| Prostate volume (ml), mean (range) | 48.29 (14.14–229.91) | 39.99 (14.14–107.55) | 56.58 (14.92–229.91) |
| PSA density(ng/ml $cm^3$), mean (range)[a] | 2.00 (0.05–4.35) | 4.51 (0.11–9.30) | 0.22 (0.04–0.24) |
| No. of clinically significant PCa lesions (%)[b] | 37 (37/84, 44.05%) | 37 (37/42, 88.10%) | NA |
| No. of clinically insignificant PCa lesions (%)[b] | 5 (5/84, 5.95%) | 5 (5/42, 11.90%) | NA |

*PSA* prostate-specific antigen, *NA* not applicable, *GS* Gleason score, *PI-RADS* prostate imaging reporting and data system

[a]The mean PSA levels are 96.41 ng/ml in All, 180.40 ng/ml in the Cancer group, and 12.42 ng/ml in the Noncancer group

[b]The definitions of clinically significant cancer (GS ≥ 3+4 = 7) and clinically insignificant cancer (GS < 7) are based on the PI-RADS v2 guideline [6]

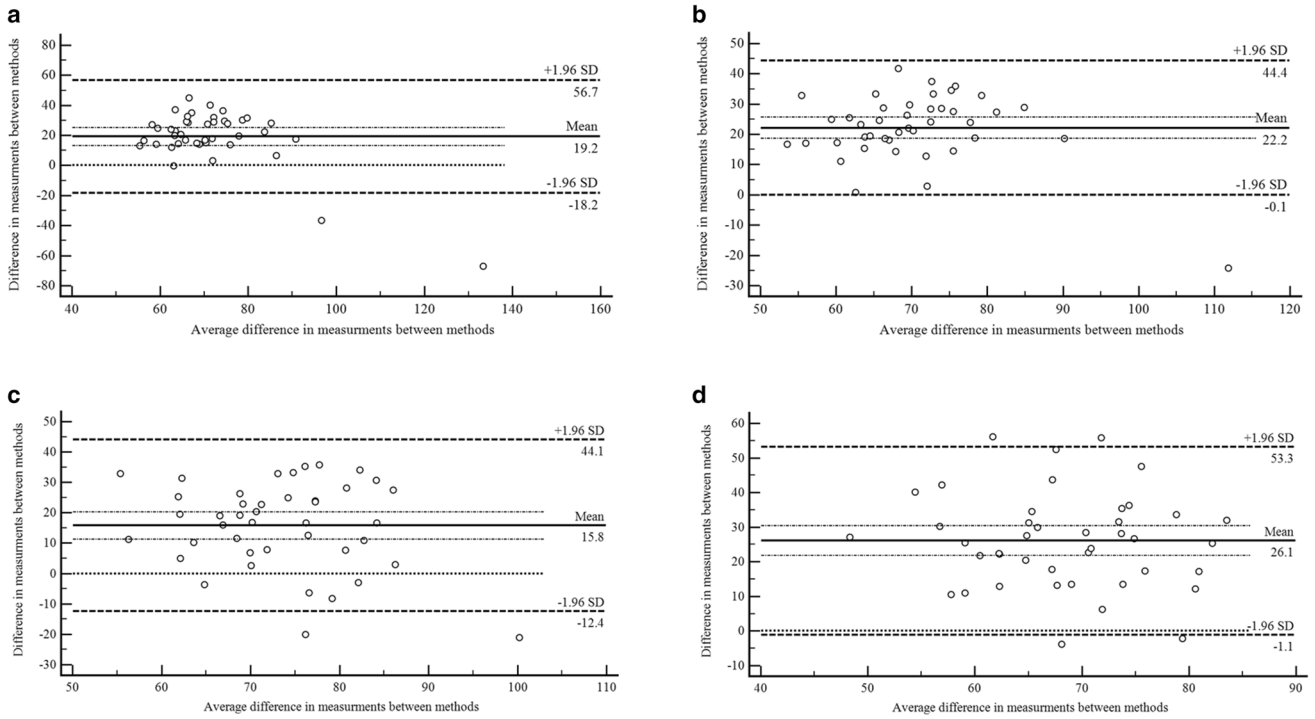


**Fig. 2** **a**–**d** images show some representative examples of Bland–Altman plots illustrating the CPMG-T2 mapping method and SE-EPI-T2 mapping method for measurements of T2 values (diff *b* values) in the cancer group. **a** $b = 20$ s/mm$^2$. **b** $b = 100$ s/mm$^2$. **C** $b = 500$ s/mm$^2$. **d** $b = 2000$ s/mm$^2$. Substantial agreement regarding the measurements was observed between the two methods, while the optimum agreement was observed at $b = 20$ and 100 s/mm$^2$. *CPMG* Carr–Purcell–Meiboom–Gill, *SE* spin echo, *EPI* echo planar imaging

## Discussion

T2 mapping can quantitatively analyze changes in the internal compositions of tissues by measuring tissue T2 values and theoretically reflect changes in tissue metabolism and biochemical information at the molecular level. T2 mapping can also detect pathological changes such as inflammation and fat infiltration, which are often observed in the musculoskeletal system [21, 22]. However, traditional T2 mapping, which is based on the CPMG method, is not widely used due to its long acquisition time (typically 5–10 min). In our previous work [17, 18] and with the current results, we proved that T2 maps generated by the SE-EPI and CPMG methods are highly correlated in prostate lesions and that the SE-EPI method has higher application value than the CPMG method. Our SE-EPI method was tested by 8 independent sessions with a total

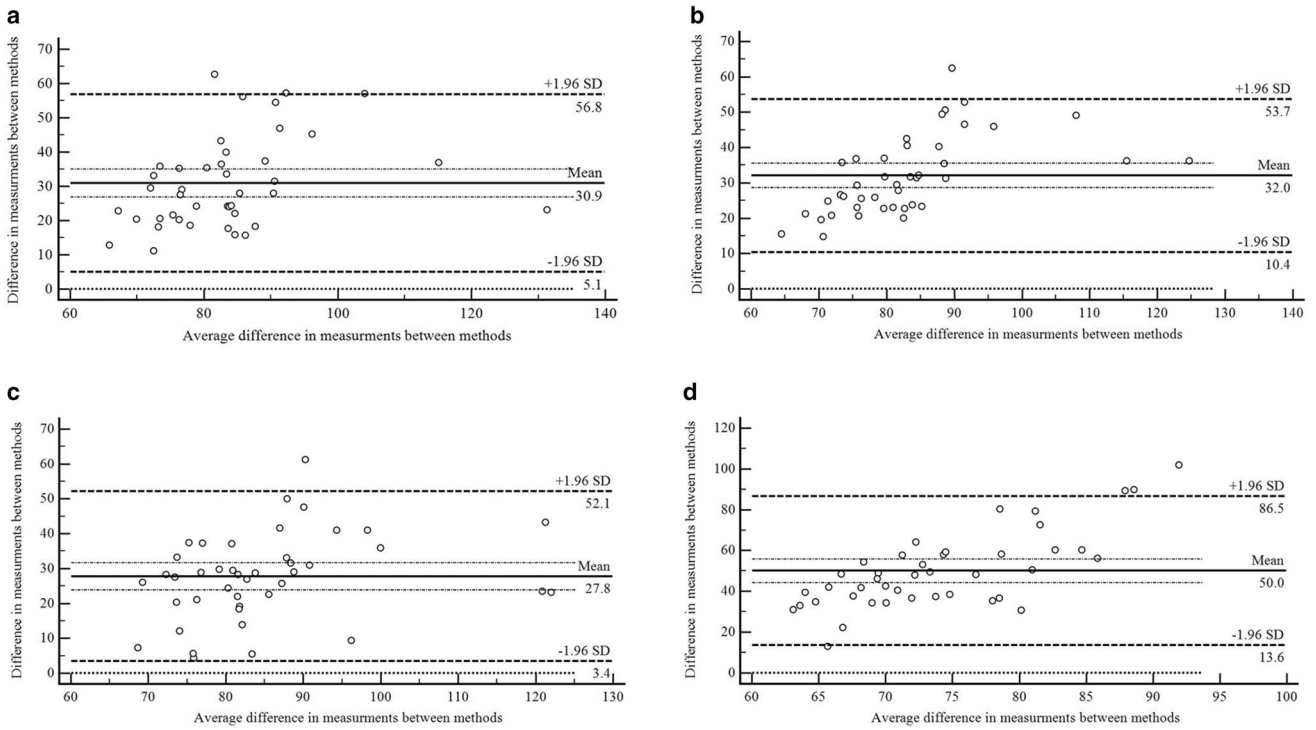


**Fig. 3** **a**–**d** images show some representative examples of Bland–Altman plots illustrating the CPMG-T2 mapping method and SE-EPI-T2 mapping method for measurements of T2 values (diff b-values) in the noncancer group. **a** $b = 20$ s/mm$^2$. **b** $b = 100$ s/mm$^2$. **c** $b = 500$ s/mm$^2$. **d** $b = 2000$ s/mm$^2$. Substantial agreement regarding the measurements was observed between the two methods, while the optimum agreement was found at $b = 20$, 100, and 500 s/mm$^2$. *CPMG* Carr–Purcell–Meiboom–Gill, *SE* spin echo, *EPI* echo planar imaging

**Table 3** The correlations of CPMG-T2 values with SE-EPI-T2 values at different b-values

| *b* value (s/mm$^2$) | Noncancer group | | Cancer group | |
|---|---|---|---|---|
| | *r* | *P* | *r* | *P* |
| 0 | 0.458 | 0.002 | 0.559 | 0.000 |
| 20 | 0.385 | 0.012 | 0.438 | 0.004 |
| 40 | 0.432 | 0.004 | 0.475 | 0.001 |
| 60 | 0.419 | 0.006 | 0.442 | 0.003 |
| 100 | 0.546 | 0.000 | 0.537 | 0.000 |
| 200 | 0.557 | 0.000 | 0.423 | 0.005 |
| 500 | 0.416 | 0.006 | 0.228 | 0.147 |
| 1000 | −0.043 | 0.788 | 0.160[a] | 0.312 |
| 2000 | −0.288 | 0.064 | 0.160[a] | 0.310 |

*CPMG* Carr–Purcell–Meiboom–Gill, *SE* spin echo, *EPI* echo planar imaging

[a]Pearson analysis was used to analyze the correlations between CPMG-T2 values and SE-EPI-T2 values at $b = 1000$ and 2000 s/mm$^2$ in the cancer group, which the data of both groups adhere to a normal distribution. And the rest of the data was analyzed using Spearman's rho analysis

acquisition time of 13 min 25 s, while each session was mostly less than 3 min, and in the future, we recommend using session 4, which exhibited better performance compared with the other sessions and saved 2–7 min compared with the traditional method. In addition, the fast acquisition of the SE-EPI method is also suitable for body organs with motion artifacts or for exams with limited scan times, where the CPMG method is not feasible. However, our study did not investigate this aspect, and the clinical value of the SE-EPI method should be studied in the future.

Additionally, SE-EPI-T2 maps can be easily incorporated into DWI scans. We can obtain T2 and ADC maps during one scan, thus enabling multiparameter analysis. Based on the results of our study, significant differences were found between the ADC (diff TE) values and T2 (diff *b*) values, which distinguished the noncancer group from the cancer group. These findings are consistent with conventional literature reports indicating that the ADC values represent the diffusion restriction of water molecules, with greater restrictions found in cancer due to the increased cell density and ratio of the intracellular nuclear plasma in tumors and the decreased values in the extracellular space. A similar result was reported by Wang et al. [16] who showed significant differences between a cancer group and a normal group in T2 values in the prostate at $b = 0$, 750 and 1500 s/mm$^2$ and in ADC values at TE = 47, 75, and 100 ms. Their results also indicated that in normal prostate ROIs, the

**Table 4** Group analysis of the T2 values (diff *b* values) and ADC values (diff TEs) based on the SE-EPI-T2 mapping method

| *b* value (s/mm$^2$) | T2 values | | | | TEs (ms) | ADC values | | | |
|---|---|---|---|---|---|---|---|---|---|
| | Noncancer group (ms) | Cancer group (ms) | Z or t[a] | *P* | | Noncancer group (μm$^2$/ms) | Cancer group (μm$^2$/ms) | Z or t[a] | *P* |
| 0 | 63.25 (56.44–95.31) | 56.47 (40.96–98.30) | − 4.893 | 0.000 | 36 | 1.42 (0.92–1.80)[b] | 1.04 (0.61–2.49) | − 5.180 | 0.000 |
| 20 | 66.33 (50.20–119.72) | 57.13 (44.04–166.90) | − 3.811 | 0.000 | 40 | 1.56 (1.15–2.65) | 1.10 (0.75–1.96) | − 6.531 | 0.000 |
| 40 | 65.78 (50.44–110.26) | 56.59 (41.42–170.23) | − 3.766 | 0.000 | 54 | 1.19 (0.77–1.52)[b] | 0.72 (0.49–1.67) | − 7.058 | 0.000 |
| 60 | 66.29 (50.85–107.82) | 59.03 (39.59–166.77) | − 3.650 | 0.000 | 69 | 0.97 (0.69–1.23)[b] | 0.61 (0.39–0.83)[b] | 15.058 | 0.000 |
| 100 | 65.19 (55.54–106.54) | 57.83 (39.03–123.91) | − 4.536 | 0.000 | 80 | 0.90 (0.66–1.17)[b] | 0.58 (0.37–0.83)[b] | 14.296 | 0.000 |
| 200 | 64.11 (55.04–98.60) | 59.47 (37.97–102.64) | − 2.809 | 0.005 | 100 | 1.01 (0.73–1.53) | 0.55 (0.12–0.85) | − 7.810 | 0.000 |
| 500 | 69.30 (56.16–110.36) | 63.93 (38.89–110.69) | − 2.254 | 0.024 | | | | | |
| 1000 | 48.07 (38.33–56.88)[b] | 56.40 (39.42–77.74)[b] | − 5.351 | 0.000 | | | | | |
| 2000 | 49.03 (38.30–64.67)[b] | 55.28 (33.57–80.47)[b] | − 3.155 | 0.002 | | | | | |

*TE* echo time, *ADC* apparent diffusion coefficient, *SE* spin echo, *EPI* echo planar imaging

[a]The two-sample t-tests was used to analyze differences between the cancerous and noncancerous groups at $b = 1000$ and 2000 s/mm$^2$, and TE = 69 and 80 ms, which the data of both groups adhere to a normal distribution. And the rest of the data was analyzed using the Mann–Whitney *U* test

[b]The original data which adhere to a normal distribution described as mean (range), while the rest of the data without "*b*" did not adhere to a normal distribution and described as median (range)

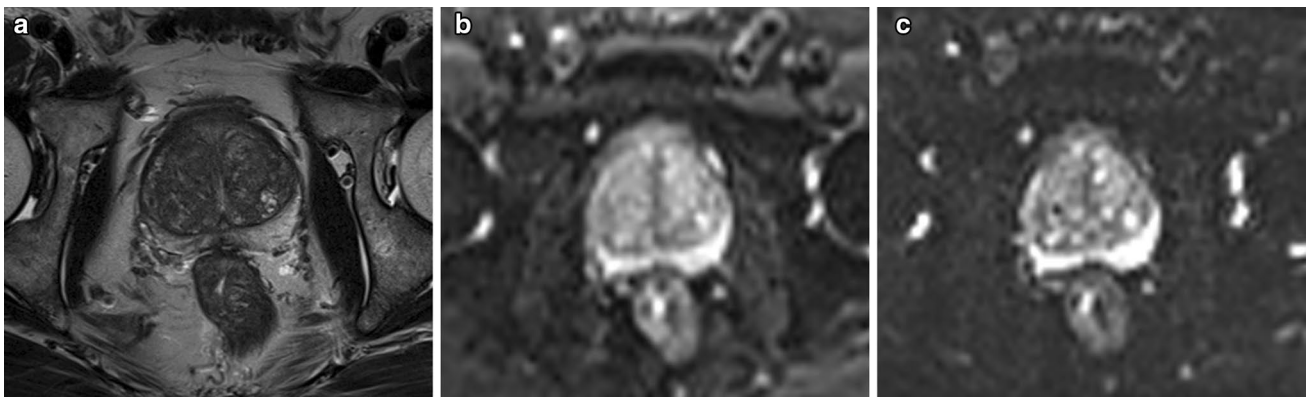


**Fig. 4** **a**–**c** derived (at the same layer) from a 62-year-old man diagnosed with BPH with a PSA level of 4.814 ng/ml. **a** T2WI image. **b** DWI image with $b = 200$ s/mm$^2$. TE = 54 ms. **c** DWI image with $b = 200$ s/mm$^2$, TE = 100 ms. At the same *b* value, the spatial resolution of each image decreases as the TE increases; however, the contrast between the TZ and PZ of the prostate was increased. *BPH* benign prostatic hyperplasia, *T2WI* T2-weighted imaging, *DWI* diffusion-weighted imaging, *TE* echo time, *TZ* transition zone, *PZ* peripheral zone, *PSA* prostate-specific antigen

ADC at TE = 47 ms was significantly lower than the ADC at TE = 100 ms ($P = 0.0003$), and the T2 value at $b = 0$ s/mm$^2$ was significantly longer than the T2 value at $b = 1500$ s/mm$^2$ ($P = 0.001$), which were the same as the results in cancer ROIs. However, in our study, the results of the ADC values at different TEs were opposite to those of Wang et al. The ADC values at TE = 69 and 80 ms were slightly lower than those at TE = 36, 40, 54, and 100 ms. This discrepancy may be explained by the small population included in the study of Wang et al., the lower TE settings, and the absence of a large range of *b* values. While the results for the T2 values at different *b* values in our study were the same as those in the study of Wang et al., i.e., the T2 values at $b = 0$ s/mm$^2$ were higher than those at $b = 1000$ and 2000 s/mm$^2$, this result may have been due to a third component, namely, blood flow [18]. The T2 relaxation time of the blood signal is relatively longer than that of other prostate tissues, including gland cells, stromal cells, and tumor cells. The blood flow or perfusion signal quickly decays when a diffusion gradient is applied; thus, only the T2 value at $b = 0$ s/mm$^2$ contained the significant signal component of perfusion and showed higher values than those at other *b* values.

In our study, when considering the optimal b-value for selection, one of the interesting phenomena observed when

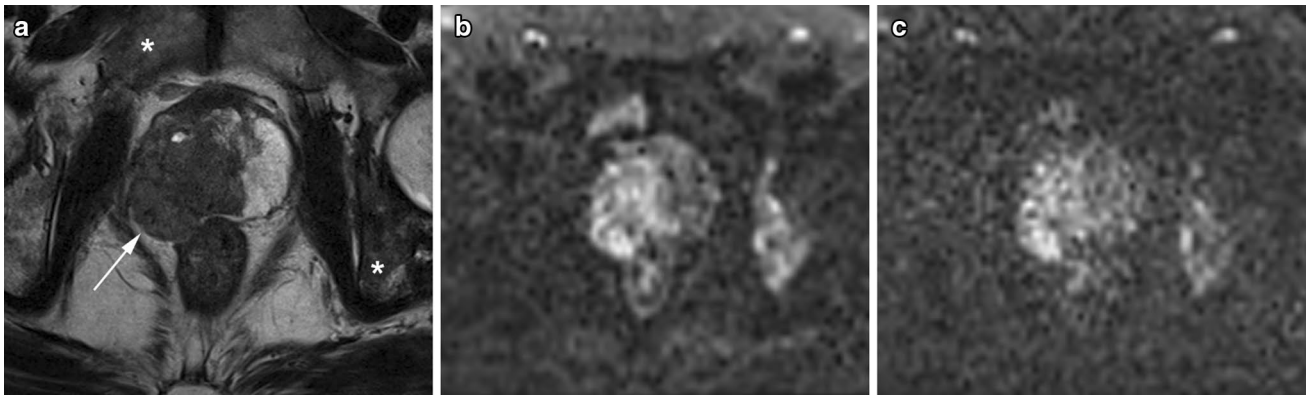


**Fig. 5** **a**–**c** derived (at the same layer) from a 65-year-old man diagnosed with PCa (right PZ and TZ, GS = 4+4 = 8) with a PSA level of 163.361 ng/ml. **a** T2WI image. **b** DWI image with $b = 1000$ s/mm$^2$, TE = 54 ms. **c** DWI image with b = 1000 s/mm$^2$, TE = 100 ms. At $b = 1000$ s/mm$^2$, good contrast of the lesion (arrow) is evident, and the bone metastases (asterisk) are clearly displayed. However, the quality of the shorter-TE image (**b**) is better than that of the longer-TE image (**c**). *PCa* prostate cancer, *T2WI* T2-weighted imaging, *DWI* diffusion-weighted imaging, *TE* echo time, *TZ* transition zone, *PZ* peripheral zone, *PSA* prostate-specific antigen, *GS* Gleason score

we performed the statistical analysis was that as the *b* values increased, the data gradually tended toward a normal distribution, especially at *b* values of 1000 and 2000 s/mm$^2$. However, as the *b* value increases, the signal-to-noise (SNR) ratio of the image and spatial resolution decreases significantly, and the image distortion is gradually increasing. Therefore, we need to include more patients with more lesions in the future to verify these results further. We also analyzed the correlations between the CPMG-T2 values and the SE-EPI-T2 values at different *b* values in both the noncancer group and the cancer group. The results showed that the average correlation between the CPMG-T2 values and the SE-EPI-T2 values was moderate in both groups, and prominent statistically significant differences were found in both the noncancer group and the cancer group ($P < 0.05$). Thus, the SE-EPI-based T2 mapping method, which required less time and allowed simultaneous calculation of multiple parameters, may be a preferable substitute for the traditional CPMG-T2 mapping method. However, no other relevant study based on the SE-EPI method has performed a similar correlation analysis; thus, unfortunately, comparison or analysis of these results must await future work.

Our study has several limitations. First, the SE-EPI method has low spatial resolution and causes image distortion, which can be improved by adopting readout-segmented-EPI or slice-specific shimming techniques. Second, the absolute T2 value of the SE-EPI method is not equivalent to that of the CPMG method due to the long echo train, but the strong correlation shown in our previous work [17, 18] and the current results indicate the feasibility of the SE-EPI method. In terms of patients, the primary limitation is that the median PSA level of the cancer group was higher than that in other studies, which may have generated a bias in the study because of the unbalanced enrollment. This limitation has been reported in other studies [23]. However, our study was not designed to evaluate diagnostic accuracy, and the PSA level was not included as a diagnostic variable. Instead, the parameters used in the calculations and analysis were determined by the sequence setting, and the goal was to determine the validity of the T2 and ADC values in differentiating benign and malignant prostate lesions based on the SE-EPI-T2 mapping method. Therefore, the higher PSA levels of the patients had little effect on the results of the study, and we hope to improve this aspect in the future. In addition, to avoid generating a bias in the analysis, the cancer group in our study was not further grouped into a clinically significant versus nonsignificant group due to the small number of clinically insignificant PCa lesions. In terms of pathology, the reference standard that we used was TRUS-guided prostate biopsies, which may be less accurate than prostatectomy specimens [24]. In addition, the final number of enrolled cases in this study was still relatively small ($n = 84$), resulting in insufficiently precise power to predict the invasiveness of PCa. To conduct further analyses and research, a larger clinical trial with more patients who have undergone prostatectomy and with a large range of GSs will be required in the future.

In conclusion, the results of this study show that SE-EPI-based T2 mapping has potential application value in PCa and can be easily used in joint analyses with ADC mapping, thus serving as a simple and quantitative method of multiparametric quantitative analysis. In addition, this technique may be considered a replacement for fast T2 mapping and can be used in moving organs or in examinations with limited scan times, where the CPMG method is not feasible.

**Acknowledgements** We thank Xu Yan and his team from the MR Collaboration NE Asia, Siemens Healthcare, for providing the scan guide and settings.

**Funding** This work was supported by the National Natural Science Foundation of China (NSFC) [Grant Numbers 81671656 and 81171307].

## Compliance with ethical standards

**Conflict of interest** Xu Yan is an employee of Siemens Healthcare but had no control over the inclusion of any data or information that might have presented a conflict of interest. There are no actual or potential conflicts of interest to declare in relation to this article. None of the other authors have conflicts of interest or specific financial interests relevant to the subject of this article.

## References


1. Siegel RL, Miller KD, Jemal A. (2018) Cancer statistics, 2018. CA Cancer J Clin 1:7-30. https://doi.org/10.3322/caac.21442
2. Mazaheri Y, Shukla-Dave A, Muellner A, Hricak H. (2011) MRI of the prostate: clinical relevance and emerging applications. J Magn Reson Imaging 2:258-274. https://doi.org/10.1002/jmri.22420
3. Turkbey B, Choyke PL. (2012) Multiparametric MRI and prostate cancer diagnosis and risk stratification. Curr Opin Urol 4:310-315. https://doi.org/10.1097/MOU.0b013e32835481c2
4. Lin WC, Westphalen AC, Silva GE, Chodraui Filho S, Reis RB, Muglia VF. (2016) Comparison of PI-RADS 2, ADC histogram-derived parameters, and their combination for the diagnosis of peripheral zone prostate cancer. Abdom Radiol (NY) 11:2209-2217. https://doi.org/10.1007/s00261-016-0826-4
5. Barentsz JO, Richenberg J, Clements R, Choyke P, Verma S, Villeirs G, et al. (2012) ESUR prostate MR guidelines 2012. Eur Radiol 22:746-757. https://doi.org/10.1007/s00330-011-2377-y
6. Weinreb JC, Barentsz JO, Choyke PL, Cornud F, Haider MA, Macura KJ, et al. (2016) PI-RADS Prostate Imaging - Reporting and Data System: 2015, Version 2. Eur Radiol 69:16-40. https://doi.org/10.1016/j.eururo.2015.08.052
7. Hoang Dinh A, Souchon R, Melodelima C, Bratan F, Mège-Lechevallier F, Colombel M, et al. (2015) Characterization of prostate cancer using T2 mapping at 3T: a multi-scanner study. Diagn Interv Imaging 4:365-372. https://doi.org/10.1016/j.diii.2014.11.016
8. Katsube T, Okada M, Kumano S, Imaoka I, Kagawa Y, Hori M, et al. (2012) Estimation of liver function using T2* mapping on gadolinium ethoxybenzyl diethylenetriamine pentaacetic acid enhanced magnetic resonance imaging. Eur J Radiol 7:1460-1464. https://doi.org/10.1016/j.ejrad.2011.03.073
9. MacKay A, Whittall K, Adler J, Li D, Paty D, Graeb D. (1994) In vivo visualization of myelin water in brain by magnetic resonance. Magn Reson Med 6:673-677. https://doi.org/10.1002/mrm.1910310614
10. Ghugre NR, Ramanan V, Pop M, Yang Y, Barry J, Qiang B, et al. (2011) Myocardial BOLD imaging at 3 T using quantitative T2: application in a myocardial infarct model. Magn Reson Med 6:1739-1747. https://doi.org/10.1002/mrm.22972
11. Hada S, Ishijima M, Kaneko H, Kinoshita M, Liu L, Sadatsuki R, et al. (2017) Association of medial meniscal extrusion with medial tibial osteophyte distance detected by T2 mapping MRI in patients with early-stage knee osteoarthritis. Arthritis Res Ther 1:201. https://doi.org/10.1186/s13075-017-1411-0
12. Kim HK, Laor T, Horn PS, Racadio JM, Wong B, Dardzinski BJ. (2010) T2 mapping in Duchenne muscular dystrophy: distribution of disease activity and correlation with clinical assessments. Radiology 3:899-908. https://doi.org/10.1148/radiol.10091547
13. Carter JS, Koopmeiners JS, Kuehn-Hajder JE, Metzger GJ, Lakkadi N, Downs LS Jr, et al. (2013) Quantitative multiparametric MRI of ovarian cancer. J Magn Reson Imaging 6:1501-1509. https://doi.org/10.1002/jmri.24119
14. Liney GP, Knowles AJ, Manton DJ, Turnbull LW, Blackband SJ, Horsman A. (1996) Comparison of conventional single echo and multi-echo sequences with a fast spin-echo sequence for quantitative T2 mapping: application to the prostate. J Magn Reson Imaging 4:603-607. https://doi.org/10.1002/jmri.1880060408
15. Glaser C. (2005) New techniques for cartilage imaging: T2 relaxation time and diffusion-weighted MR imaging. Radiol Clin North Am 4:641-653, vii. https://doi.org/10.1016/j.rcl.2005.02.007
16. Wang S, Peng Y, Medved M, Yousuf AN, Ivancevic MK, Karademir I, et al. (2014) Hybrid multidimensional T(2) and diffusion-weighted MRI for prostate cancer detection. J Magn Reson Imaging 4:781-788. https://doi.org/10.1002/jmri.24212
17. Yan X, Ke Z, Zhou MX, Fu CX, Min XD, Wang L. (2017) Application of fast SE-EPI-based T2 mapping in prostate, with comparison to conventional CPMG-based T2 mapping. Proceedings of the 25th Annual Meeting of ISMRM; 2017 Apr 22-27; Honolulu, Hawaii, United States. Concord (CA): ISMRM Press; 2017. Abstract: 3418. https://indexsmart.mirasmart.com/ISMRM2017/PDFfiles/3418.html#_parent
18. Zhou MX, Ke Z, Min XD, Wang L, Ma C, Yan X. (2017) Validation of fast SE-EPI T2 mapping with reference to conventional CPMG T2 mapping, and its application in prostate cancer. Proceedings of the 10th International Congress on Image and Signal Processing, BioMedical Engineering and Informatics (CISP-BMEI); 2017 Oct 14-16; Shanghai, China. New York (NY): IEEE Press; 2018. Pages: 1-5. https://doi.org/10.1109/CISP-BMEI.2017.8302183
19. Barbieri S, Bronnimann M, Boxler S, Vermathen P, Thoeny HC. (2017) Differentiation of prostate cancer lesions with high and with low Gleason score by diffusion-weighted MRI. Eur Radiol 27:1547–1555. https://doi.org/10.1007/s00330-016-4449-5
20. Baco E, Ukimura O, Rud E, Vlatkovic L, Svindland A, Aron M, et al. (2015) Magnetic resonance imaging-transectal ultrasound image-fusion biopsies accurately characterize the index tumor: correlation with step-sectioned radical prostatectomy specimens in 135 patients. Eur Urol 67:787–794. https://doi.org/10.1016/j.eururo.2014.08.077
21. Yan D, Zhang J, Liang W, Sun J, Liu BY, Tian W, et al. (2013) Magnetic resonance imaging and histopathological analysis of experimental muscle injuries in a rabbit. Biomed Environ Sci 10:841-848. https://doi.org/10.3967/bes2013.007
22. Kim HK, Laor T, Horn PS, Wong B. (2010) Quantitative assessment of the T2 relaxation time of the gluteus muscles in children with Duchenne muscular dystrophy: a comparative study before and after steroid treatment. Korean J Radiol 3:304-311. https://doi.org/10.3348/kjr.2010.11.3.304
23. Feng ZY, Wang L, Min XD, Wang SG, WangGP, Cai J. (2016) Prostate Cancer Detection with Multiparametric Magnetic Resonance Imaging: Prostate Imaging Reporting and Data System Version 1 versus Version 2. Chin Med J 129:2451-2459. https://doi.org/10.4103/0366-6999.191771
24. Siddiqui MM, Rais-Bahrami S, Truong H, Stamatakis L, Vourganti S, Nix J, et al. (2013) Magnetic resonance imaging/ultrasound-fusion biopsy significantly upgrades prostate cancer versus systematic 12-core transrectal ultrasound biopsy. Eur Urol 5:713-719. https://doi.org/10.1016/j.eururo.2013.05.059